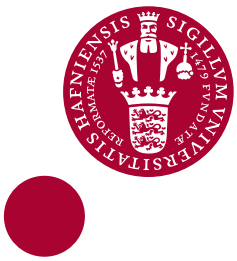

Bio-optical properties and radiative energy budgets in fed and unfed scleractinian corals (Pocillopora sp.) during thermal bleaching

Heidelberg Lyndby, Niclas; Holm, Jacob Boiesen; Wangpraseurt, Daniel; Ferrier-Pagès, Christine; Kühl, Michael

Published in:
Marine Ecology - Progress Series

DOI:
10.3354/meps13146

Publication date:
2019

Document version
Publisher's PDF, also known as Version of record

Vol. 629: 1–17, 2019
https://doi.org/10.3354/meps13146

MARINE ECOLOGY PROGRESS SERIES
Mar Ecol Prog Ser

Published October 24

FEATURE ARTICLE

Bio-optical properties and radiative energy budgets in fed and unfed scleractinian corals (*Pocillopora* sp.) during thermal bleaching

Niclas Heidelberg Lyndby[1,2,*], Jacob Boiesen Holm[1], Daniel Wangpraseurt[1,3,4], Christine Ferrier-Pagès[5], Michael Kühl[1,6]

[1]Marine Biological Section, Department of Biology, University of Copenhagen, Strandpromenaden 5, 3000 Helsingør, Denmark
[2]Laboratory for Biological Geochemistry, School of Architecture, Civil and Environmental Engineering, Ecole Polytechnique Fédérale de Lausanne, 1015 Lausanne, Switzerland
[3]Department of Chemistry, University of Cambridge, CB2 1EW Cambridge, UK
[4]Scripps Institution of Oceanography, 9500 Gilman Drive, La Jolla, California 92093, USA
[5]Centre Scientifique de Monaco, Coral ecophysiology team, 8 Quai Antoine 1er, 98000 Monaco
[6]Climate Change Cluster, University of Technology, Ultimo, NSW 2007, Australia

ABSTRACT: Corals live in symbiosis with algal dinoflagellates, which can achieve outstanding photosynthetic energy efficiencies *in hospite* approaching theoretical limits. However, how such photosynthetic efficiency varies with environmental stress remains poorly known. Using fiber-optic and electrochemical microsensors in combination with variable chlorophyll fluorescence imaging, we investigated the combined effects of thermal stress and active feeding on the radiative energy budget and photosynthetic efficiency of the symbiotic coral *Pocillopora* sp. At ambient temperature (25°C), the percentage of absorbed light energy used for photosynthesis under low irradiance was higher for fed (~5–6%) compared to unfed corals (4%). Corals from both feeding treatments responded equally to stress from high light exposure (2400 µmol photons m^{-2} s^{-1}), exhibiting a decrease in photosynthetic efficiency, down to 0.5–0.6%. Fed corals showed increased resilience to thermal-induced bleaching (loss of symbionts) compared to unfed corals. In addition, while unfed corals decreased their photosynthetic efficiency almost immediately when exposed to thermal stress, fed corals maintained a constant and high photosynthetic efficiency for 5 more days after onset of thermal stress. We conclude that active feeding is beneficial to corals by prolonging coral health and resilience during thermal stress as a result of an overall healthier symbiont population.

KEY WORDS: Coral bleaching · Feeding · Symbiosis · Microsensors · Light scattering · Photobiology

*Corresponding author: niclas.lyndby@epfl.ch

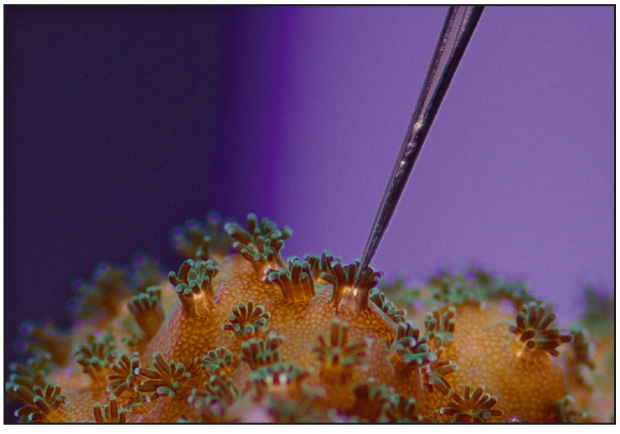

Microsensor measuring oxygen production at the base of a single polyp of *Pocillopora damicornis*.

Photo: Niclas H. Lyndby

1. INTRODUCTION

Tropical coral reefs are among the most diverse and productive ecosystems on Earth, although they occur in oligotrophic waters. The key drivers of reef formation are hermatypic scleractinian corals, which are fueled by various genera of endosymbiotic dinoflagellate microalgae belonging to the family Symbiodiniaceae (previously referred to as the single genus *Symbiodinium*; LaJeunesse et al. 2018). The coral holobiont, i.e. the association of the coral polyp

Publisher: Inter-Research · www.int-res.com

with the Symbiodiniaceae and microbes in coral tissue and skeleton (Bourne et al. 2009), is able to acquire nutrients both via heterotrophy (e.g. prey capture; Houlbrèque & Ferrier-Pagès 2009) and autotrophy (via symbiont photosynthesis and subsequent translocation of photosynthates from the symbionts to the host; Muscatine et al. 1981). While the dinoflagellate symbionts, i.e. zooxanthellae, only represent ~5–15% of the coral tissue biomass (Odum & Odum 1955, Thornhill et al. 2011), they provide up to 95% of the coral's energetic carbon demand (Muscatine et al. 1981, Edmunds & Davies 1989). However, corals are susceptible to environmental stress (e.g. changes in seawater temperature, eutrophication, sedimentation or salinity), which can lead to the breakdown of the coral–algal symbiosis and the expulsion of the symbiotic algae, a phenomenon known as coral bleaching (Lesser 1996, Hoegh-Guldberg 1999, Hoegh-Guldberg et al. 2007, Wiedenmann et al. 2013).

Mass bleaching events have increased in frequency due to global climate change-derived heating of the ocean surface waters, which now represents a major threat to coral reefs worldwide (Hoegh-Guldberg 1999, Hughes et al. 2003, 2017, Ainsworth et al. 2016). On a larger scale, the most widely acknowledged stressors are instances of above-average sea water temperatures due to global warming, in combination with excess solar irradiance (Glynn 1996). The primary biochemical causes of coral bleaching are still debated (Brown & Dunne 2015) but are strongly linked to the formation of reactive oxygen species (ROS) in corals upon environmental stress (Lesser 1996, Bou-Abdallah et al. 2006). Irradiance exposure plays a central role in the bleaching response of corals, and excess irradiance can lead to photodamage of photosystem II and essential repair systems in the zooxanthellae leading to the production of ROS (Lesser 1996, Lesser & Farrell 2004, Hill et al. 2011). Nutrient starvation can also alter the lipid composition of algal membranes, leading to photodamage and reduced chlorophyll content and photosynthesis, especially at excess temperatures (Wiedenmann et al. 2013). However, heterotrophic feeding decreases coral bleaching susceptibility (Ferrier-Pagès et al. 2010). A better understanding of how corals handle light, and how nutrition interacts with light acquisition, is thus important for a mechanistic description of coral bleaching.

In reef environments, fluctuations in irradiance exposure (ranging from seconds to hours) create a need for regulating and optimizing light harvesting and utilization of incident light energy in symbiont-bearing corals (Anthony & Hoegh-Guldberg 2003, Veal et al. 2010a). Photon absorption and the light microenvironment in corals are strongly modulated by the optical properties of the coral tissue and skeleton (Enriquez et al. 2005, Wangpraseurt et al. 2012, 2014a, Marcelino et al. 2013). The density and distribution of coral host pigments and symbionts in the tissue, as well as the scattering properties of both coral tissue and skeleton, are important factors for modulating symbiont light absorption and thus photosynthetic efficiency *in hospite* (Wangpraseurt et al. 2014b, 2019, Gittins et al. 2015, Lyndby et al. 2016). Photons traveling through coral tissue can undergo several scattering events, leading to localized scalar irradiance enhancement in upper tissue layers (Kühl et al. 1995, Wangpraseurt et al. 2012, 2017a). While such enhancement in light exposure contributes to high rates of photosynthesis of corals under optimal irradiance exposure (Brodersen et al. 2014), the same light-enhancing mechanisms can cause stress when corals are subject to excess irradiance, eventually resulting in coral bleaching. Enhanced skeletal scattering during bleaching leads to enhanced light absorption by the remaining dinoflagellate cells and can thus induce further light stress, ultimately accelerating the bleaching response, in a process known as the optical feedback loop (Enriquez et al. 2005, Wangpraseurt et al. 2017a).

Furthermore, the absorption of light energy is a major driver of radiative heat generation in coral tissue (Jimenez et al. 2012), with the rate of coral heating being directly proportional to the amount of incident light energy (Jimenez et al. 2008, Welch & van Gemert 2011). Excess heat from the tissue is dissipated via convection into the surrounding water across a thermal boundary layer (TBL), and via heat conduction down into the coral skeleton (Jimenez et al. 2008). The thickness of the TBL changes depending on the ambient flow regime and coral topography (analogous to the well-known diffusive boundary layer, DBL), while the coral tissue surface area/volume ratio affects overall coral surface warming and cooling (Jimenez et al. 2008, 2011). Coral surface topography thus affects the properties of the flow-dependent DBL and TBL, ultimately controlling the exchange of solutes and heat (Lesser et al. 1994, Kaandorp et al. 1996, Jimenez et al. 2008, Chan et al. 2016).

Studies of photosynthetic efficiency and radiative energy budgets accounting for the fate of incident and absorbed light energy in benthic marine systems have so far focused on sediments, biofilms,

and microbial mats (Al-Najjar et al. 2010, 2012, Lichtenberg et al. 2017), with the exception of a single study on a symbiont-bearing coral showing that light is used very efficiently for photosynthesis in corals (Brodersen et al. 2014). It was found that while the majority (>96%) of incident light energy was absorbed and dissipated as heat, the local photosynthetic energy efficiency of zooxanthellae in the tissue of corals measured under low to moderate irradiance approached the theoretical maximum of 0.125 mol O_2 per mol photons. Furthermore, Brodersen et al. (2014) showed that as they increased the incident irradiance, the proportion of photosynthesis in the radiative energy budget decreased and heat dissipation increased, while reflectance (%) remained unchanged at about 10% of the incident irradiance. Similar observations have been made in microbial mats, although these systems exhibit a much lower photosynthetic efficiency (Al-Najjar et al. 2010).

In this study, we investigated the closed radiative energy budgets in fed and unfed corals of *Pocillopora* sp. during thermal bleaching. This was based on detailed microsensor measurements of light, temperature and photosynthesis, and variable chlorophyll fluorescence imaging.

2. MATERIALS AND METHODS

2.1. Corals

Nubbins of *Pocillopora* sp. (presumed *P. damicornis*) were prepared by cutting 8 mother colonies into 128 fragments of 2–3 cm in diameter (16 fragments per colony), which were hung from nylon threads in several glass aquaria. Two months in advance of the bleaching experiment, the 16 fragments per colony were further divided into 8 fed or unfed nubbins, themselves equally divided into 4 fed and unfed tanks (2 nubbins per colony and per tank). All nubbins were kept under white light (250 W metal halide lamps), at a downwelling photon irradiance (400–700 nm) of 250 ± 20 µmol photons m^{-2} s^{-1}, illuminated for 12 h d^{-1}. As aquaria were in transparent glass, and the set up was placed on a highly reflective white bench, light reaching the nubbins was not significantly different between the upper and lower side of the nubbins. Fed corals were fed once a day with ~4000 *Artemia* nauplii per coral fragment, 4 times per week, and unfed corals were heterotrophically starved throughout the study, including the 2 mo prior to measurements.

At the beginning of the study, all 8 tanks started at 25°C. One tank per feeding treatment was then kept as a control, while the 3 other tanks were used for exposing corals to thermal stress by gradually ramping water temperature up to 30°C over a period of 5 d, at a rate of 1°C d^{-1}. Thermally stressed corals were kept at 30°C for an additional 2 to 3 d before starting measurements. Corals measurements after 2–3 d of 30°C thermal stress are denoted as time point 1 (T_1). After an additional 5 d of thermal stress, measurements were conducted again, denoted as time point 2 (T_2). Measurements on control corals were done during the time period between T_1 and T_2, and are denoted time point 0 (T_0). No measurements were performed on unfed corals after 8 d of stress (T_2) due to significant bleaching, which impaired measurements.

2.2. Experimental setup and approach

Microsensor measurements were performed on corals placed in a black acrylic flow chamber, which was supplied with seawater (25°C, salinity 35 ppt) from a heated water reservoir (10 l) at a flow rate of ~0.25 cm s^{-1}. A motorized micromanipulator (MU-1, PyroScience) was attached to a heavy duty stand to facilitate positioning of microsensors on fragments at a 45° angle relative to the vertically incident light. A digital microscope (Dino-Lite Edge AM7515MZTL, AnMo Electronics) was used for observation, while carefully positioning microsensor tips onto the coral tissue surface (Fig. 1e,f). Corals were illuminated from above with white light provided by a tungsten halogen lamp with an internal heat filter (KL-2500 LCD, Schott), fitted with a fiber light guide and a collimating lens (Fig. S1 in the Supplement at www.int-res.com/articles/suppl/m629p001_supp.pdf). A calibrated spectroradiometer (MSC-15, GigaHertz-Optik) was used to quantify the absolute downwelling photon irradiance (photosynthetically active radiation, PAR, 400–700 nm) at different lamp settings (80, 167, 250, 480, 970, and 2400 µmol photons m^{-2} s^{-1}), and to record downwelling irradiance spectra in units of W m^{-2} nm^{-1}. The irradiance was adjusted without changing spectral composition by adjusting a metal disk with varying perforation between the halogen light bulb and the fiber-optic light guide in the lamp light path. Setups were covered with black cloth during measurements to avoid stray light. For each coral replicate used in this study, microsensor measurements were done on 3 randomly chosen polyps located on the branch tips (Fig. 1).

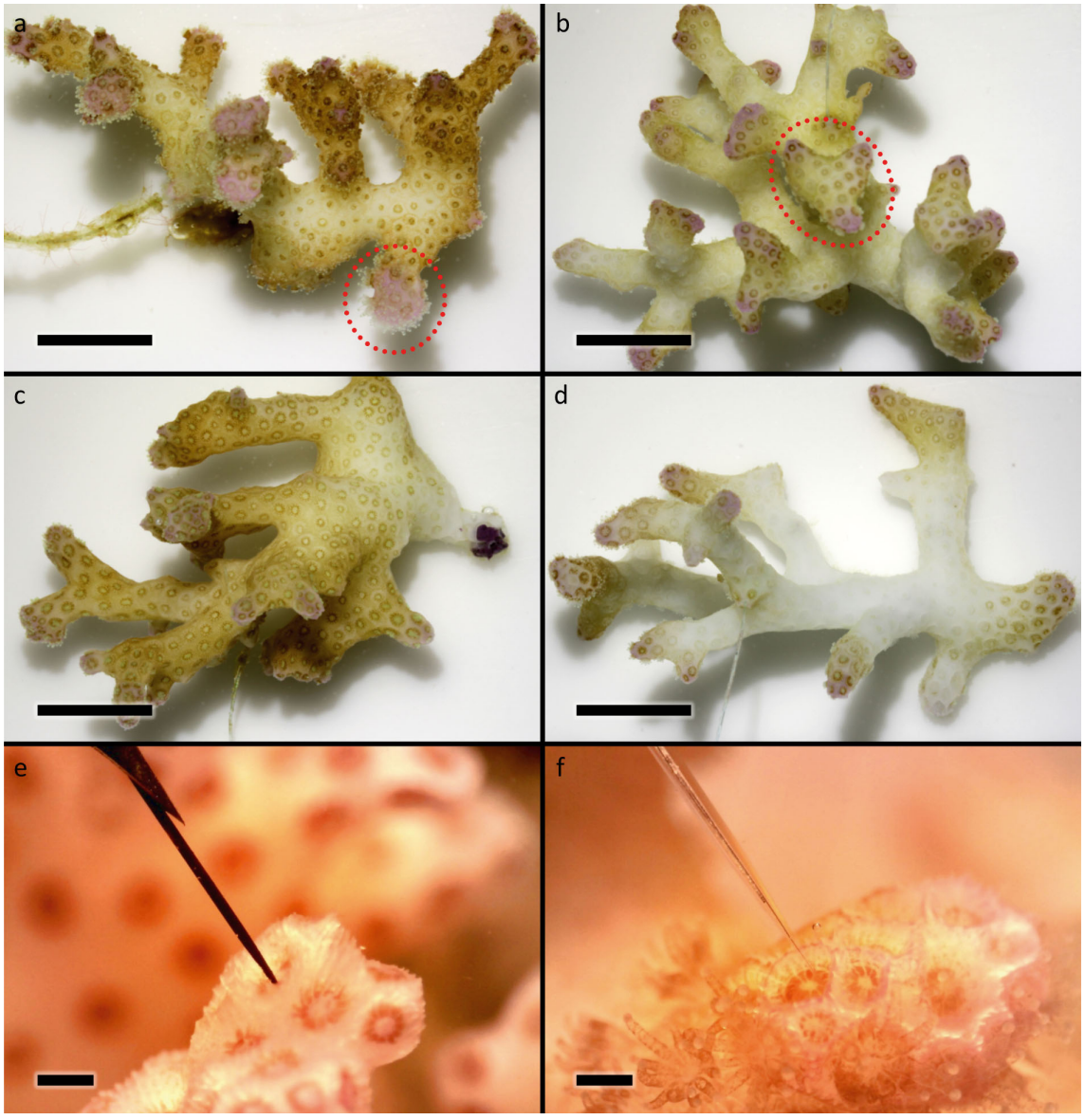

Fig. 1. Representative photographs of *Pocillopora* sp. corals subject to 4 experimental treatments: (a,b) controls and (c,d) thermally stressed fragments of fed (a,c) and unfed (b,d) *Pocillopora* sp. Photos were taken at the end of the experimental period, on the last day of measurements on unfed fragments (T_1). (e,f) Close-ups of measuring areas, with scalar irradiance (e) and O_2 (f) microsensors positioned on polyp tissue. The sensor tips were aimed at the highly pigmented polyp rims located at the branch tips of fragments. All photos were normalized against a white standard by adjusting the brightness/contrast levels using ImageJ. Note that the coral animal tissue structure was intact for all fragments. Sale bars = 1 cm (panels a–d) and 2.5 mm (panels e,f). Red dotted circles in panels a and b indicate examples of areas used for microsensor measurements

2.3. Microsensor measurements

2.3.1. Scalar irradiance and reflectance measurements

Spectral scalar irradiance was measured with a fiber-optic scalar irradiance microsensor (spherical tip diameter ~50 µm; Rickelt et al. 2016). Measurements were performed at the tissue surface and within the coral tissue for corals with tissue thicker than 50 µm. Tissue thick enough (>50 µm) was carefully punctured with a tungsten needle (tip diameter ~1 µm, see Wangpraseurt et al. 2017b for details), after which the sensor tip was quickly moved into the tissue. A reference spectrum of the incident downwelling irradiance was measured afterwards without the coral fragment and with the scalar irradiance microsensor tip placed over a black light well at the

same position in the flow chamber and incident collimated light field as the coral surface.

Light reflection (arbitrary unit; counts) of the coral tissue surface was measured with a 0.7 mm wide flat-cut fiber-optic probe positioned at a distance of 500 µm from the tissue surface. To obtain the irradiance reflectance (in % of incident irradiance), all measurements were normalized with the reflected light from a 99% white diffusing reflectance standard (Spectralon, Labsphere) measured under identical configuration to measurements at the coral surface but performed in air with the same distance from the tungsten halogen lamp (KL 2500, Schott).

Both scalar irradiance and reflectance microprobes were oriented at 45° relative to the vertically incident light and were connected to a fiber-optic spectrometer (USB 2000+, Ocean Optics). All spectra were recorded with the software SpectraSuite (version 2.0.162, Ocean Optics) running on a PC connected to the spectrometer via a USB cable.

2.3.2. Photosynthesis and O_2 measurements

Gross photosynthesis was measured with Clark-type O_2 microelectrodes with a tip diameter of ~25 µm, a low stirring sensitivity (2–3%), and a fast response time (<0.5 s; OX-25 fast, Unisense). The microelectrodes were connected to a pA meter (Unisense), and were linearly calibrated from readings in 100% air-saturated seawater and anoxic water (by addition of Na_2SO_3) at experimental temperature and salinity. The corresponding O_2 concentration (µmol l^{-1}) in seawater at 100% air saturation was taken from gas tables for the O_2 solubility in air-saturated water as a function of temperature and salinity (www.unisense.com). Data were recorded on a strip-chart recorder (BD25, Kipp&Zonen) connected to the pA meter. Gross photosynthesis was estimated using the light-dark shift method as described in detail by Revsbech & Jørgensen (1983), where the measurements performed at the coral tissue surface were regarded as representative of the entire tissue volume of *Pocillopora* sp. given that the tissue thickness in most places was less than 100–200 µm, which approximates the spatial resolution of the light–dark shift method during the 2–3 s period of darkening. Accordingly, the areal rate of gross photosynthesis was estimated by multiplying the measured volume-specific gross photosynthesis at the tissue surface (in nmol O_2 cm^{-3} s^{-1}) by the local tissue thickness (in cm). The local tissue thickness was estimated from the difference in depth position of the scalar irradiance measurements done at the water–tissue and tissue–skeleton interface, respectively.

2.3.3. Temperature measurements

Coral tissue surface heating was measured with a temperature microsensor (tip diameter ~50 µm; TP50, Unisense) connected to a thermocouple meter (T301, Unisense). The thermocouple meter was interfaced to a PC via an A/D converter (DCR 16, PyroScience) connected to a PC running the software Profix (version 4.51, PyroScience) that controlled the positioning of the micromanipulator and data acquisition. The temperature microsensor was linearly calibrated against a high-precision thermometer (Testo 110) in seawater at 19 and 25°C. Temperature profiles were measured from the tissue surface into the ambient water in steps of 100–300 µm (with a resting time of 7 s at each depth position) across the TBL (Jimenez et al. 2008). The thickness of the TBL was determined as the intersection of the linear part of the temperature profile and the ambient water (cf. Fig. 1b in Jimenez et al. 2008). ΔT was determined as the temperature difference in °C between the coral surface and ambient water outside the TBL (i.e. 5 mm above the tissue surface). All temperature measurements were done under a high incident photon irradiance (400–700 nm) of 2400 µmol photons m^{-2} s^{-1}.

2.4. Chlorophyll content and symbiont density

Chlorophyll a+c_2 content and symbiont density were determined for 4–5 coral fragments from each treatment at each time point. For this, tissue was first detached using a Water Pick with filtered seawater (FSW, 0.45 µm pore size). The tissue slurry was then homogenized using a Potter tissue grinder. For chlorophyll content determination, 5 ml of the homogenate were centrifuged at 11 000 × g (15 min at 4°C); the supernatant was discarded and the remaining algal pellet was re-suspended in 5 ml of pure acetone. Pigments were extracted at 4°C over a period of 24 h in darkness, before they were centrifuged. The pigment-containing supernatant was collected, and the chlorophyll content was determined by the spectrophotometric method of Jeffrey & Humphrey (1975) using a spectrophotometer (UVmc2, Safas).

The density of *Cladocopium* sp. (formerly *Symbiodinium* clade C; LaJeunesse et al. 2018) was determined by centrifugation of 0.1 ml of the tissue homogenate at 850 × g (10 min). The supernatant was

discarded, and the algal pellet was re-suspended in FSW that was subsequently used for 10 separate chamber counts. *Cladocopium* sp. were counted according to the method described by Rodolfo-Metalpa et al. (2006) using image analysis software (Histolab 5.2.3, Microvision Instruments).

Values of chlorophyll content and symbiont density were normalized against the skeleton surface area of the individual coral fragments as determined by the wax dipping method described by Veal et al. (2010b).

2.5. Imaging of variable chlorophyll fluorescence and absorptivity

The absorptivity and PSII quantum yield of randomly selected fragments from both control tanks T_0, unfed T_1, and fed T_2 were measured using a variable chlorophyll fluorescence imaging system using red measuring and actinic light (I-PAM, IMAG-MIN/R, Walz; Ralph et al. 2005). The measuring light intensity was adjusted for each measurement to yield an F_0 value (see Table 1) of about 0.1 for each sample.

Data were collected by placing 3–4 fragments from one treatment and time point in a clear glass container filled with seawater from the holding tank. Fragments were dark-acclimated for 15 min in seawater tanks covered with dark cloths before transfer in dim light to the PAM fluorometer followed by 5 min of further dark acclimation. After a total of 20 min of dark acclimation, the maximal PSII quantum yield (F_v/F_m) was measured by applying a strong saturation pulse (>3000 µmol photons m^{-2} s^{-1} for 0.8 s) with the imaging PAM:

$$F_v/F_m = (F_m - F_0)/F_m \quad (1)$$

where F_0 denotes the minimum fluorescent yield under dark acclimation, and F_m denotes the maximal fluorescent yield under complete closure of PSII during the saturation pulse.

Rapid light curves (RLCs) were measured for actinic light intensities ranging between 0 and 1600 µmol photons m^{-2} s^{-1}. For each RLC, corals were exposed to a total of 14 light intensities (12, 40, 73, 99, 132, 162, 190, 292, 437, 606, 853, 1177, 1631 µmol photons m^{-2} s^{-1}) for 10 s at each light intensity. The effective PSII quantum yield, Y(II), quantum yield of regulated energy dissipation, Y(NPQ), and quantum yield of nonregulated energy dissipation, Y(NO), were calculated as:

$$Y(\text{II}) = (F_m' - F)/F_m' \quad (2)$$

$$Y(\text{NPQ}) = 1 - Y(\text{II}) - 1/[\text{NPQ} + 1 + qL(F_m/F_0 - 1)] \quad (3)$$

$$Y(\text{NO}) = 1/[\text{NPQ} + 1 + qL(F_m/F_0 - 1)] \quad (4)$$

$$Y(\text{II}) + Y(\text{NPQ}) + Y(\text{NO}) = 1 \quad (5)$$

where F denotes the fluorescent yield in the presence of actinic light, F_m' denotes the maximum fluorescent yield during a saturation pulse, and qL is the fraction of PSII reaction centers that are open. See Hill et al. (2004) and Baker (2008) for more details on variable chlorophyll fluorimetry. Calculations were performed for defined tissue areas by selecting regions of interest using the software ImagingWin (v2.41a, Walz). See Table 1 for definitions of parameters used.

2.6. Radiative energy budget calculations

The radiative energy budget was calculated following procedures described in detail by Al-Najjar et al. (2010) but with minor changes as described below. The absolute downwelling spectral irradiance (in W m^{-2} nm^{-1}) was measured with a calibrated spectroradiometer (MSC15, GigaHertz-Optik) and integrated over 400–700 nm (PAR) to quantify the total incident radiant energy flux of PAR (J_{IN}, J m^{-2} s^{-1}).

From J_{IN}, we estimated the proportion of light energy absorbed (J_{abs}) and reflected (R) by the coral. The PAR irradiance reflectance (%; $R_{(PAR)}$) was calculated as:

$$R_{(PAR)} = R_t/R_{ws} \quad (6)$$

where R_t is the reflected light from coral tissue, and R_{ws} is the reflected light measured from a 99% white diffusing standard (Spectralon, Labsphere). The upwelling reflected light energy (R; in J m^{-2} s^{-1}) was calculated as:

Table 1. Definitions of parameters used for imaging of variable chlorophyll fluorescence

Parameter	Definition
F_m	Maximal fluorescence yield (dark adapted)
F_0	Minimal fluorescence yield (dark adapted)
F_v/F_m	Maximal PSII quantum yield
F_m'	Maximum fluorescence yield (light acclimated)
F	Fluorescence yield (light acclimated)
qL	Fraction of PSII centers that are open
Y(II)	Effective PSII quantum yield
Y(NPQ)	Quantum yield of regulated energy dissipation
Y(NO)	Quantum yield of nonregulated energy dissipation

$$R = J_{IN} \times R_{(PAR)} \quad (7)$$

The light energy absorbed by the coral tissue, J_{abs} (in J m^{-2} s^{-1}), was then calculated as the vector irradiance:

$$J_{abs} = J_{IN} \times (1 - R_{(PAR)}) \quad (8)$$

The absorbed light energy in the coral is either dissipated as heat, J_H, or conserved by photosynthesis, J_{PS}. The energy conserved by photosynthesis was estimated by recalculating the measured areal gross photosynthesis, GPP, in energy units by multiplication with the Gibbs free energy, E_G = 482.9 kJ $(mol\ O_2)^{-1}$, i.e. the amount of energy produced during oxygenic photosynthesis (Al-Najjar et al. 2010). The total amount of energy conserved by photosynthesis, J_{PS} (in J m^{-2} s^{-1}) was thus calculated as:

$$J_{PS} = GPP \times E_G \quad (9)$$

The remaining part of the absorbed light was dissipated as heat, J_H, via an upward heat flux across the TBL or via a downward heat flux into the coral skeleton (Jimenez et al. 2008). The upward heat flux, $J_{H\text{-}up}$, was calculated from temperature microsensor measurements across the TBL, using the linear slope of the temperature profile (K m^{-1}) over the coral tissue surface, and multiplying it with the thermal conductivity of seawater at a salinity of 35 ppt, k = 0.6 W m^{-1} K^{-1}:

$$J_{H\text{-}up} = k \frac{dT}{dz} \quad (10)$$

where T is the temperature measured in Kelvin, and z is the distance measured in m. It was not possible to directly measure the heat conduction from tissue into the coral skeleton with the fragile temperature microsensors, and the downward heat flux, $J_{H\text{-}down}$ (in J m^{-2} s^{-1}) was thus estimated as:

$$J_{H\text{-}down} = J_{abs} - (J_{H\text{-}up} + J_{PS}) \quad (11)$$

The total amount of energy dissipated as heat in the coral, J_H (in J m^{-2} s^{-1}), was then calculated as:

$$J_H = J_{H\text{-}up} - J_{H\text{-}down} \quad (12)$$

The entire radiative energy budget (in J m^{-2} s^{-1}) is thus found as:

$$J_{IN} = J_{abs} - R = J_{PS} + J_H - R \quad (13)$$

Energy budgets at lower irradiances were calculated based on detailed gross photosynthesis measurements on fragments from all time points (T_0–T_2) at previously mentioned photon irradiances (see Section 2.2). The detailed measurements were combined with temperature and reflectance data, based on the assumption of a positive linear relationship between incident downwelling photon irradiance and heat dissipation (Jimenez et al. 2008), and a near-constant percentage of reflection from the coral surface regardless of the incident irradiance (Al-Najjar et al. 2010, Brodersen et al. 2014). See Table 2 for definitions and units of abbreviations and parameters used.

3. RESULTS

3.1. Variable chlorophyll fluorescence imaging

The effective PSII quantum yield, Y(II), at the incident downwelling irradiance (E_d = 1630 µmol photons m^{-2} s^{-1}) in unfed corals did not change over time from (T_0) and during thermal stress (T_1), while fed corals showed a significant 3.2-fold increase of Y(II) after 8 d at 30°C (T_2) relative to the control treatment (ANOVA, $F_{1,46}$ = 12.7, p << 0.01; Fig. 2a). Overall, fed corals presented a higher Y(II) than unfed corals during all measurements (Fig. 2a).

The maximal relative PS electron transport rate, rETR, at the highest photon irradiance (E_d = 1630 µmol photons m^{-2} s^{-1}) did not differ between unfed corals before (T_0) and after thermal stress (T_1), while fed corals showed a significant 1.6-fold increase in rETR after 8 d at 30°C (T_2) relative to the

Table 2. Abbreviations, definitions, and units used for the radiative energy budget calculations. N/A: not applicable

Abbreviation	Definition	Unit
PAR	Photosynthetically active radiation (400–700 nm)	N/A
TBL	Thermal boundary layer	N/A
R_t	Tissue reflected light	Arbitrary unit
R_{ws}	Reflected light from white standard reflectance	Arbitrary unit
$R_{(PAR)}$	PAR irradiance reflectance (R_t / R_{ws})	Arbitrary unit
J_{IN}	Downwelling irradiance in energy units	J m^{-2} s^{-1}
R	Reflected light energy	J m^{-2} s^{-1}
J_{abs}	Absorbed light energy	J m^{-2} s^{-1}
GPP	Areal rate of gross primary production	nmol O_2 cm^{-2} s^{-1}
E_G	Gibbs energy	kJ $(mol\ O_2)^{-1}$
J_{PS}	Energy conserved by photosynthesis	J m^{-2} s^{-1}
k	Thermal conductivity of seawater	W m^{-1} K^{-1}
dT/dz	Temperature gradient in the TBL	K $µm^{-1}$
$J_{H\text{-}up}$	Upward heat flux in energy units	J m^{-2} s^{-1}
$J_{H\text{-}down}$	Downward heat flux in energy units	J m^{-2} s^{-1}
J_H	Total heat flux in energy units	J m^{-2} s^{-1}

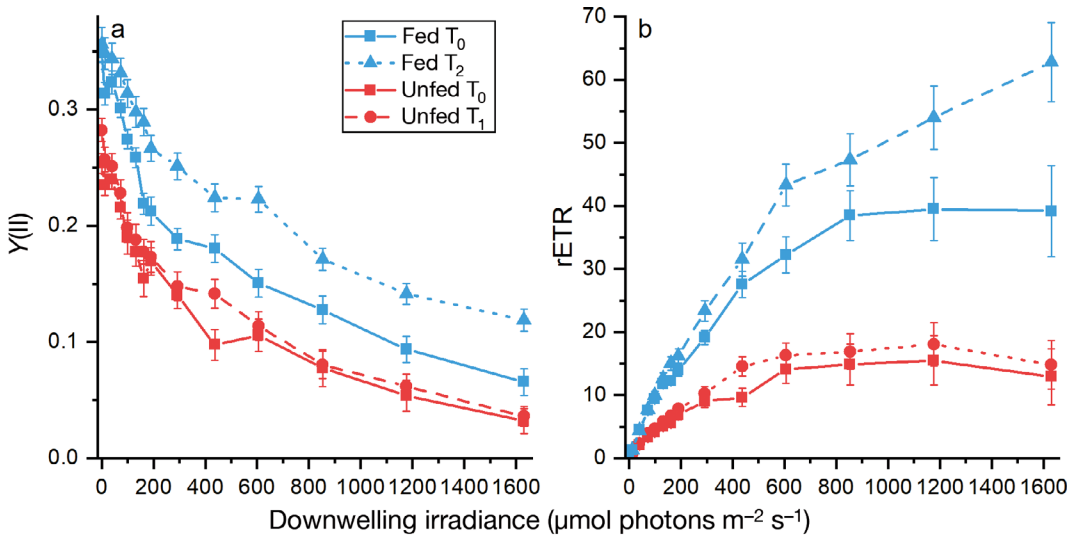

Fig. 2. Variable chlorophyll fluorescence imaging of polyp tissue in fed and unfed *Pocillopora* sp. during thermal stress treatment. (a) Effective PSII quantum yield [*Y*(II)], and (b) relative electron transport rate (rETR) before (T_0) and after thermal stress (T_1–T_2). Symbols with error bars indicate means ± SE of *Y*(II) and rETR in different areas of interest in the images (n = 24–36)

control (T_0, ANOVA, $F_{1,46}$ = 6.1, p = 0.02; Fig. 2b). The rETR of fed corals was also 2-fold higher than the rETR of unfed corals, at both T_0 and T_1, and all light levels, which is in agreement with a higher F_v/F_m (ANOVA, $F_{1,106}$ = 44.3, p << 0.01; see F_v/F_m data in Fig. S2).

3.2. Chlorophyll content and symbiont density

Cladocopium sp. cell density at T_0 was about 1.9 times higher for fed fragments compared to unfed fragments (ANOVA, $F_{1,7}$ = 74.8, p << 0.01), and cell density decreased steadily in corals under both feeding treatments during thermal stress (T_1–T_2, Fig. 3a). Relative to the starting population at T_0, cell density loss in fed fragments was 10.1 % after 3 d at 30°C (T_1), and 27.5 % after 8 d at 30°C (T_2; ANOVA, $F_{2,11}$ = 6.2, p = 0.016). For unfed fragments, cell density loss was 23.4 % after 3 d at 30°C (T_1), relative to the starting population (ANOVA, $F_{1,7}$ = 9.1, p = 0.020; Fig. 3a). The chlorophyll content per area (µg cm^{-2}) was about 3.4 times higher in fed fragments as compared to unfed fragments at T_0 (ANOVA, $F_{1,21}$ = 17.8, p << 0.01). No significant changes in chlorophyll (µg cm^{-2}) were observed during thermal stress in fragments from both feeding treatments relative to the starting content (T_0–T_2; ANOVA, $F_{2,11}$ = 0.8, p = 0.49 for fed, $F_{1,7}$ = 0.3, p = 0.61; Fig. 3b).

Chlorophyll content per cell was not affected by thermal stress relative to the starting content, but was on average 1.8 times higher in *Cladocopium* sp. from fed fragments compared to *Cladocopium* sp. from unfed fragments across all time points (T_0–T_2; ANOVA, $F_{1,3}$ = 49.1, p < 0.01; Fig. 3c).

3.3. Scalar irradiance

Coral tissue surface photon scalar irradiance (425–700 nm) at T_0 was 122.7 ± 0.07 % (mean ± SE) of the incident downwelling photon irradiance (E_d = 2400 µmol photons m^{-2} s^{-1}) pooled across fed and unfed corals with no significant difference between the 2 groups (ANOVA, $F_{1,25}$ = 0.24, p = 0.63; Fig. 4a). Enhancement of tissue surface scalar irradiance peaked after 3 d at 30°C (T_1) in both treatments, reaching a pooled photon scalar irradiance of 143.7 ± 0.07 % for both fed and unfed corals relative to E_d, with no significant differences (ANOVA, $F_{1,19}$ = 0.16, p = 0.69; Fig. 4a). At T_0, scalar irradiance at the coral tissue–skeleton interface was 98.7 ± 0.06 %of the incident downwelling irradiance pooled across fed and unfed corals with no significant difference between the 2 groups (ANOVA, $F_{1,23}$ = 0.51, p = 0.48; Fig. 4b). Scalar irradiance at the tissue–skeleton interface did not change with thermal stress (T_1–T_2) relative to T_0 (ANOVA, $F_{2,34}$ = 1.5, p = 0.24 for fed, $F_{1,21}$ = 2.8, p = 0.19 for unfed; Fig. 4b).

A distinct spectral attenuation was observed in the near infrared part of the spectrum (700–750 nm) at the tissue–skeleton interface in unfed corals after 3 d at 30°C (T_1), and in fed corals after 8 d at 30°C (T_2; Fig. 4e,f), suggestive of the presence of endoliths in the coral skeleton, but no such endoliths were perceivable to the naked eye (see Section 4.1).

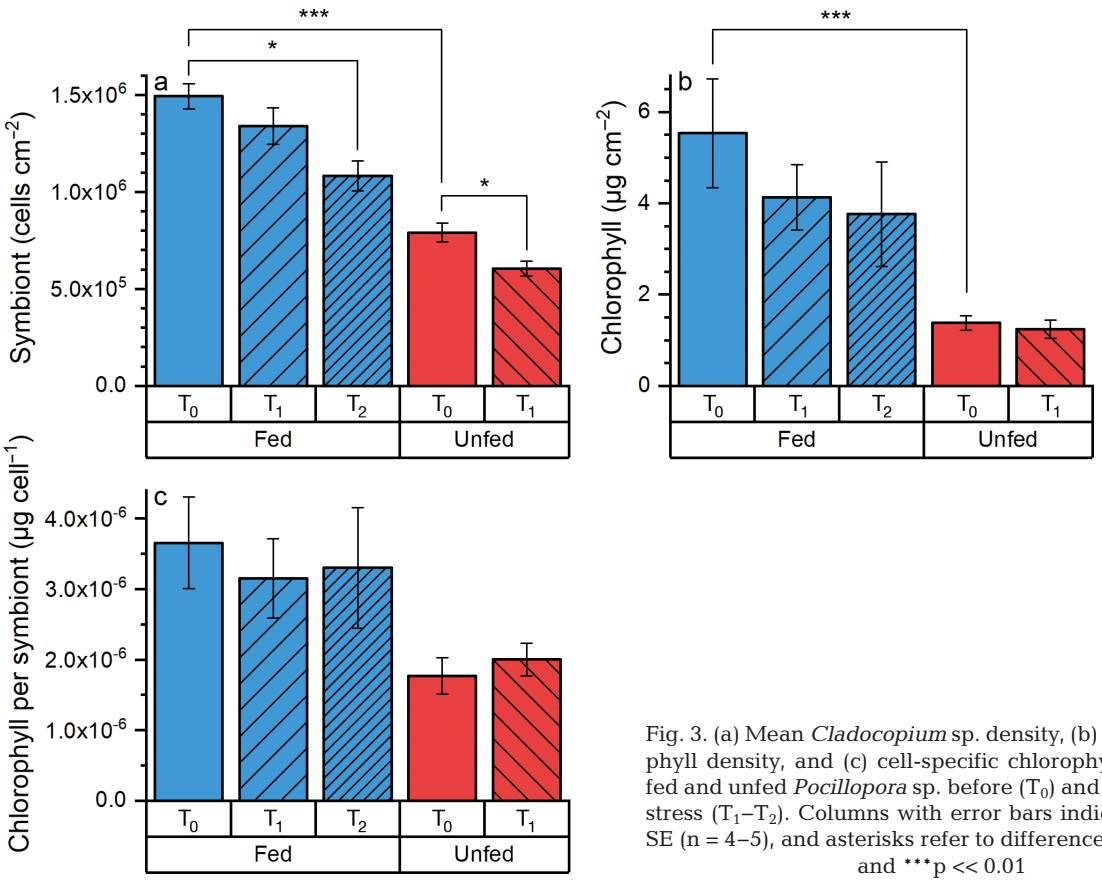

Fig. 3. (a) Mean *Cladocopium* sp. density, (b) mean chlorophyll density, and (c) cell-specific chlorophyll content in fed and unfed *Pocillopora* sp. before (T_0) and after thermal stress (T_1–T_2). Columns with error bars indicate means ± SE (n = 4–5), and asterisks refer to differences at $^*p < 0.05$ and $^{***}p << 0.01$

3.4. Reflectance measurements

Spectral reflectance (%) of PAR (400–700 nm) was 11.7 ± 0.009(SE)% and 15.5 ± 0.007 % at T_0 for fed and unfed fragments of *Pocillopora* sp., respectively (Fig. 5a). Fed coral fragments showed a significantly increased reflectance (%) at T_2, relative to control measurements (T_2; ANOVA, $F_{1,37}$ = 6.2, p = 0.018), while unfed fragments showed no significant increase in reflectance (%) between T_0 and T_1 (ANOVA, $F_{1,34}$ = 0.6, p = 0.46; Fig. 5a). Reflectance (%) spectra from both fed and unfed fragments showed the lowest reflection in areas of absorption maxima for chl *a* (435–440 and 675 nm), the peridinin-chlorophyll-protein complex (540 nm), and chl *c* (630–635 nm; Fig. 5b,c).

3.5. Gross photosynthesis

Areal gross photosynthesis rates measured at high incident photon irradiance of E_d = 2400 µmol photons m^{-2} s^{-1} were not statistically different between measurements performed at any time point or feeding treatment (ANOVA, $F_{2,19}$ = 1.4, p = 0.26 for fed, and $F_{1,22}$ = 1.1, p = 0.30 for unfed; Fig. 6a).

For fed fragments, mean gross photosynthesis per cell was 1.4 times higher at T_1 relative to control fragments at T_0. No difference was observed for fed fragments between T_1 and T_2. For unfed fragments, gross photosynthesis per cell was 1.1-fold higher for T_1 compared to T_0 (Fig. 6b). Unfed fragments had an overall ~0.25–0.3 times higher gross photosynthesis per cell compared to fed fragments across all time points (Fig. 6b).

Gross photosynthesis versus photon irradiance curves were corrected for the actual *in vivo* photon scalar irradiance measured with microsensors at the coral tissue surface for the individual treatments and time points (see Section 2.3 for details). Areal gross photosynthesis for unfed control corals reached saturation level (maximal photosynthesis; P_{max}) at P_{max} = 0.52 ± 0.01(SE) nmol O_2 cm^{-2} s^{-1} (α [photosynthetic efficiency] = 0.0013 ± 0.0006 [SE]; T_0) at a photon scalar irradiance of ~2150 µmol photons m^{-2} s^{-1} (Fig. 7b). Fed control corals reached a similar saturation level at P_{max} = 0.53 ± 0.01 nmol O_2 cm^{-2} s^{-1} (α = 0.0020 ± 0.0011; T_0) at a photon scalar irradiance of ~2300 µmol photons m^{-2} s^{-1} (Fig. 7a). P_{max} for

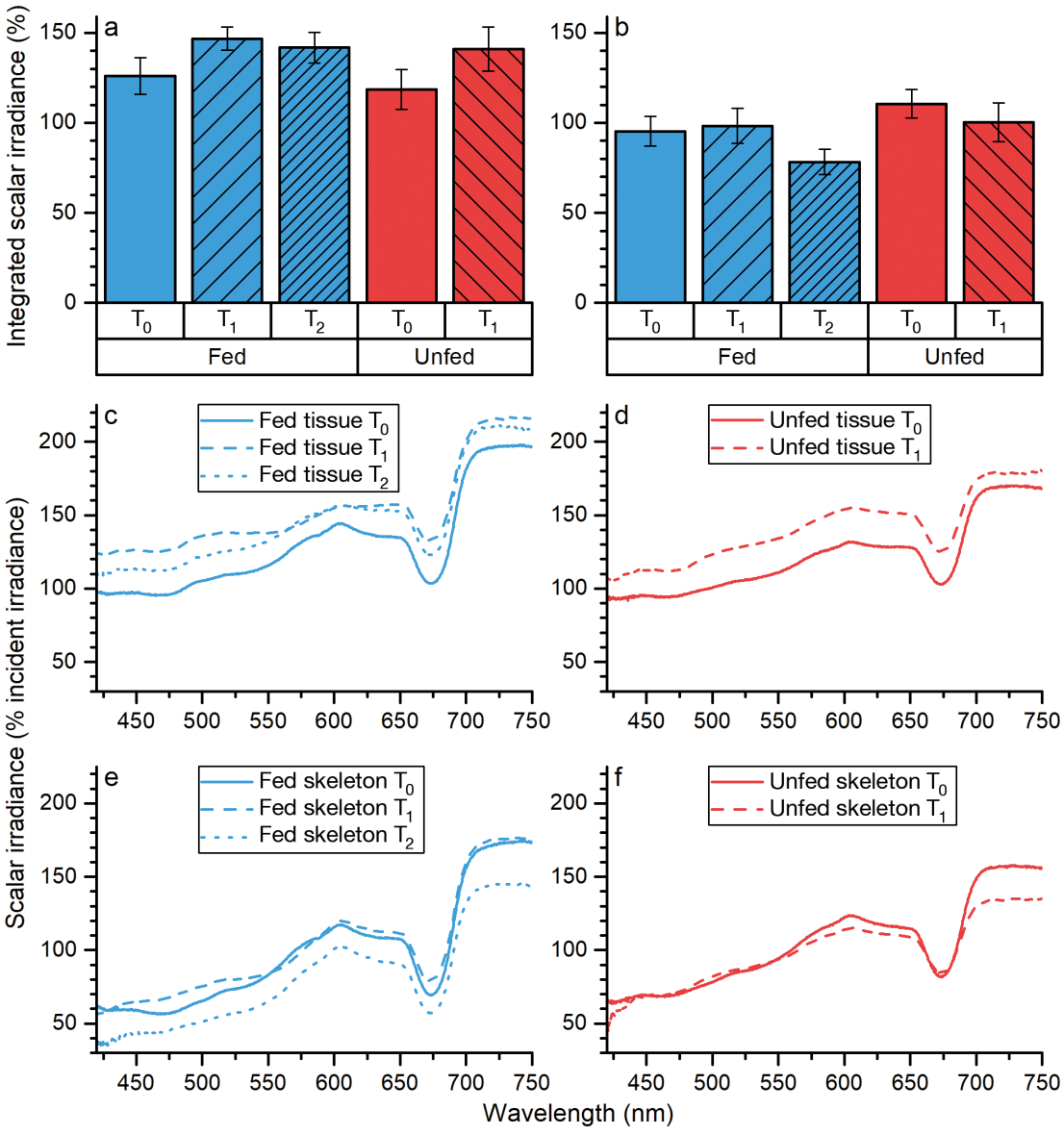

Fig. 4. (a,b) Scalar irradiance (integrated over 425–700 nm) in percent of downwelling irradiance at (a) the coral tissue surface and (b) the coral tissue–skeleton interface of fed and unfed *Pocillopora* sp. during thermal stress, and (c–f) spectral scalar irradiance (in percent of the incident downwelling irradiance) measured in (c,d) polyp surface tissue and (e,f) at the coral skeleton–tissue interface of (c,e) fed and (d,f) unfed fragments of *Pocillopora* sp. during thermal stress. Columns with error bars and all spectra indicate means ± SE (n = 10–15) for each time point per treatment (relative error of 20–50% for all spectra; c–f). Wavelengths below 425 nm were omitted due to high amounts of stray light in the spectrometer. Note that error bars in panels c–f are omitted for clarity, and the y-axes start at 30%

unfed corals dropped to 0.44 ± 0.02 nmol O_2 cm^{-2} s^{-1} (α = 0.0007 ± 0.0007; T_1), while P_{max} for fed corals increased to 0.67 ± 0.03 nmol O_2 cm^{-2} s^{-1} (α = 0.0019 ± 0.0017; T_1) after 3 d of thermal stress, under a photon scalar irradiance of ~2600 µmol photons m^{-2} s^{-1} (Fig. 7b). P_{max} decreased to 0.50 ± 0.03 nmol O_2 cm^{-2} s^{-1} (α = 0.0012 ± 0.0014; T_2) for fed corals after 8 d of thermal stress and reached saturation at ~2200 µmol photons m^{-2} s^{-1} (Fig. 7a).

3.6. Temperature measurements

The TBL thickness of *Pocillopora* sp. was 746 ± 67(SE) µm for fed fragments and 617 ± 37 µm for unfed fragments under an incident photon irradiance of E_d = 2400 µmol photons m^{-2} s^{-1} and a flow velocity of ~0.25 cm s^{-1} (Fig. 8a). For both fed and unfed fragments, surface heating at T_0 reached a ΔT of 0.19 ± 0.02(SE)°C and 0.17

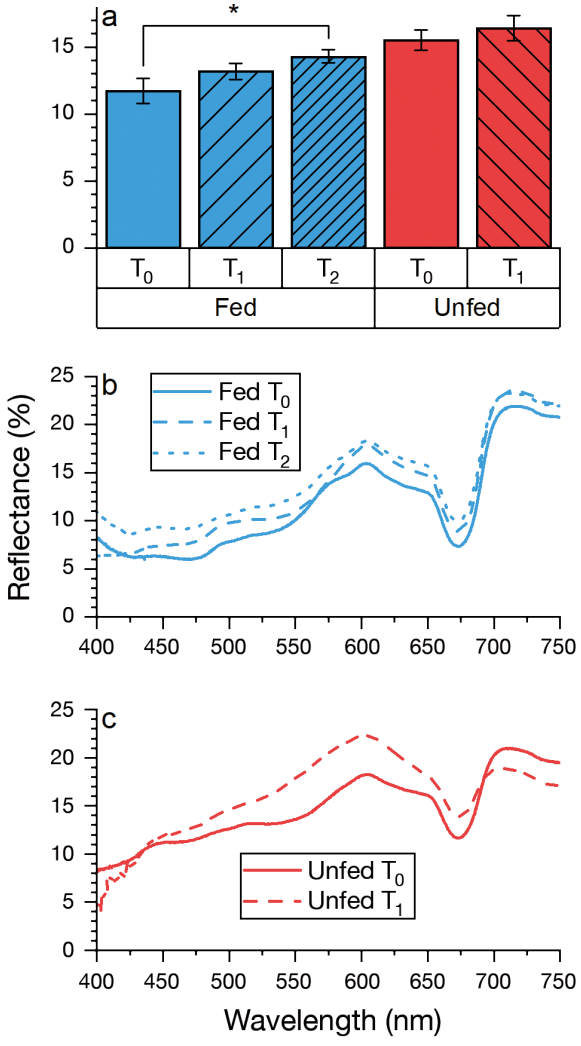

Fig. 5. (a) Diffuse reflectance of photosynthetically active radiation (PAR, integrated between 400 and 700 nm) and (b,c) spectral reflectance of fed and unfed *Pocillopora* sp. during thermal stress. Columns with error bars, and spectra indicate means ± SE (n = 9–23). Note that error bars in panels b and c are omitted for clarity (SE < 3%; n = 9–24), and asterisk refers to difference at *p < 0.05

± 0.02°C for fed and unfed corals, respectively (Fig. 8b).

3.7. Radiative energy budget

We calculated radiative energy budgets based on microsensor measurements of reflection, gross photosynthesis, and temperature for an incident downwelling photon irradiance of 2400 mol photons m^{-2} s^{-1}, which was equivalent to an incident irradiance (J_{in}) of 485.68 J m^{-2} s^{-1}.

The amount of energy lost by tissue surface reflection increased with thermal stress, thus decreasing the amount of light absorbed by the coral tissue. For fed corals, reflected light energy was 11.72% (of the incident irradiance) at T_0, 13.17% at T_1, and 14.38% at T_2. Likewise, reflectance (%) increased in unfed corals from 15.01% of incident irradiance at T_0 to 16.41% at T_1 (Fig. 9a). Under high irradiance, photosynthesis accounted for only 0.65 ± 0.05% (n = 3) and 0.57 ± 0.05% (n = 2) of the absorbed light energy in fed and unfed corals, respectively. We found no major differences in the amount of light energy conserved by photosynthe-

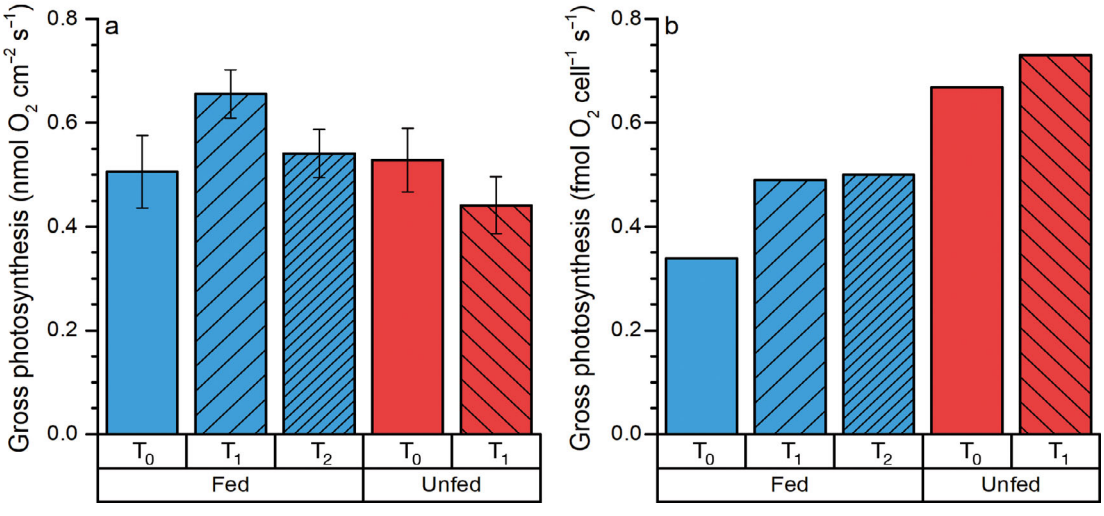

Fig. 6. (a) Areal gross photosynthesis of fed and unfed specimens of *Pocillopora* sp. under thermal stress measured at 2400 µmol photons m^{-2} s^{-1}, averaged for each time point per treatment. Columns with error bars indicate means ± SE (n = 5–12). (b) Cell-specific gross photosynthesis in fed and unfed *Pocillopora* sp. for each treatment and time point

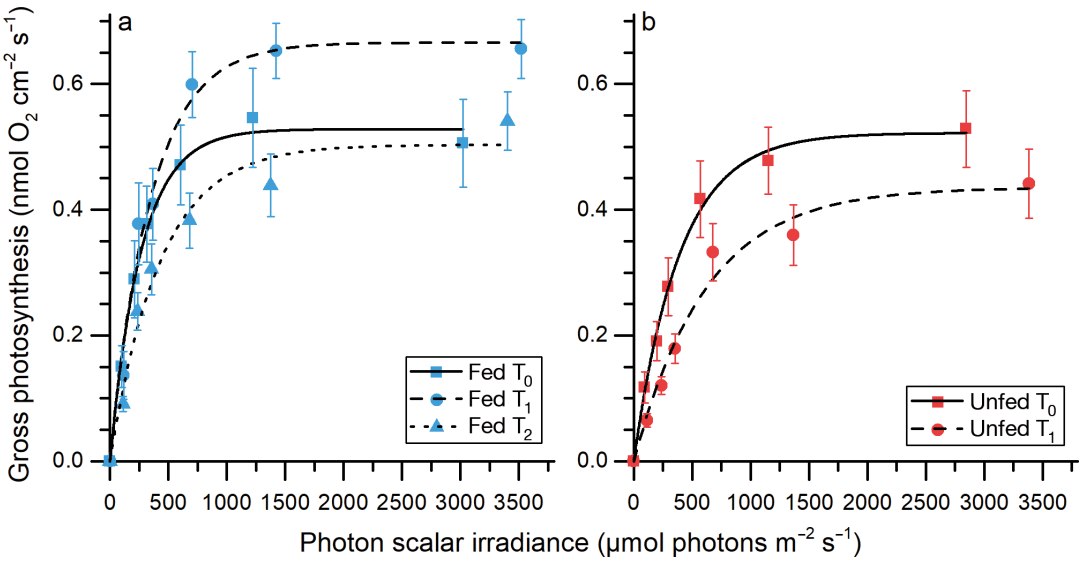

Fig. 7. Gross photosynthesis versus photon scalar irradiance (photosynthetically active radiation, PAR, 400–700 nm) curves for (a) fed and (b) unfed fragments of *Pocillopora* sp. under thermal stress. Curves represent curve fits of an exponential model (Webb et al. 1974; $R^2 > 0.97$). The light levels represent the actual amount of photons available for the individual time point and treatment by multiplying the downwelling irradiance with the local PAR enhancement obtained from the respective integrated scalar irradiance values (see Fig. 4a). Error bars indicate ± SE of the mean (n = 5–12)

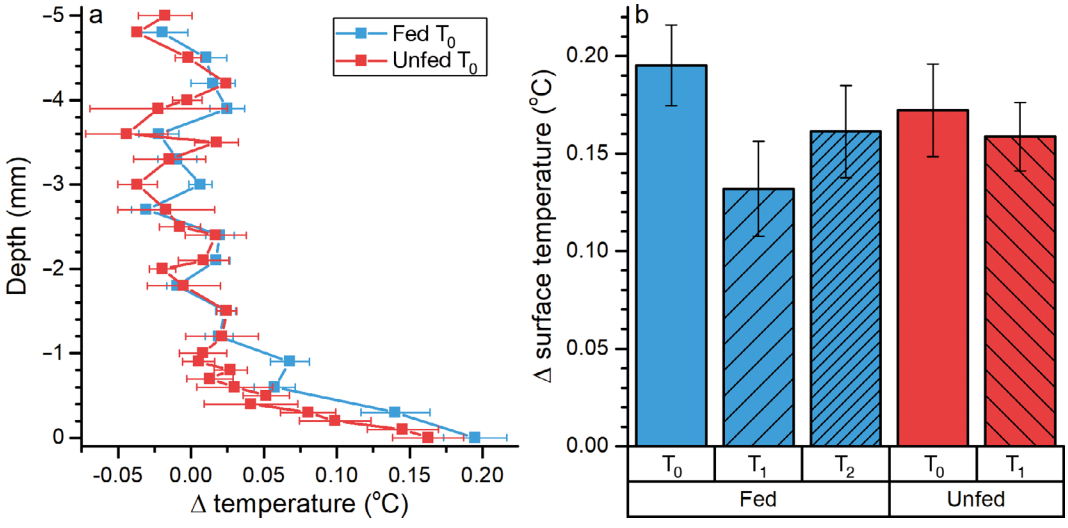

Fig. 8. (a) Temperature profiles measured towards the tissue surface of fed and unfed control fragments of *Pocillopora* sp. (at time point T_0, see T_1–T_2 in Fig. S3 in the Supplement). The *x*-axis shows the temperature difference between the coral tissue surface (0 mm) and the mean ambient water temperature under a downwelling photon irradiance of 2400 µmol photons m^{-2} s^{-1}. Symbols with error bars indicate means ± SE (n = 9–15). (b) Mean temperature differences between the coral polyp tissue surface and the ambient water at 2400 µmol photons m^{-2} s^{-1}. Columns with error bars indicate means ± SE (n = 9–15)

sis, J_{PS}, before and after thermal stress in either fed or unfed fragments (Fig. 9b), and heat dissipation, J_H, thus accounted for >99% of the absorbed energy dissipation in both fed and unfed fragments under high irradiance (Fig. 9b).

We calculated a theoretical radiative energy budget for a range of incident photon irradiance levels (from 80 to 2400 µmol photons m^{-2} s^{-1}) based on detailed gross photosynthesis measurements on control fragments performed at these light levels (see Section 2.2.). These extrapolated radiative energy budgets indicated that an increasing amount of light energy could be conserved by photosynthesis in both fed and unfed fragments, as the incident irradiance decreased, and light saturation of photosynthesis was alleviated (Fig. 10). In

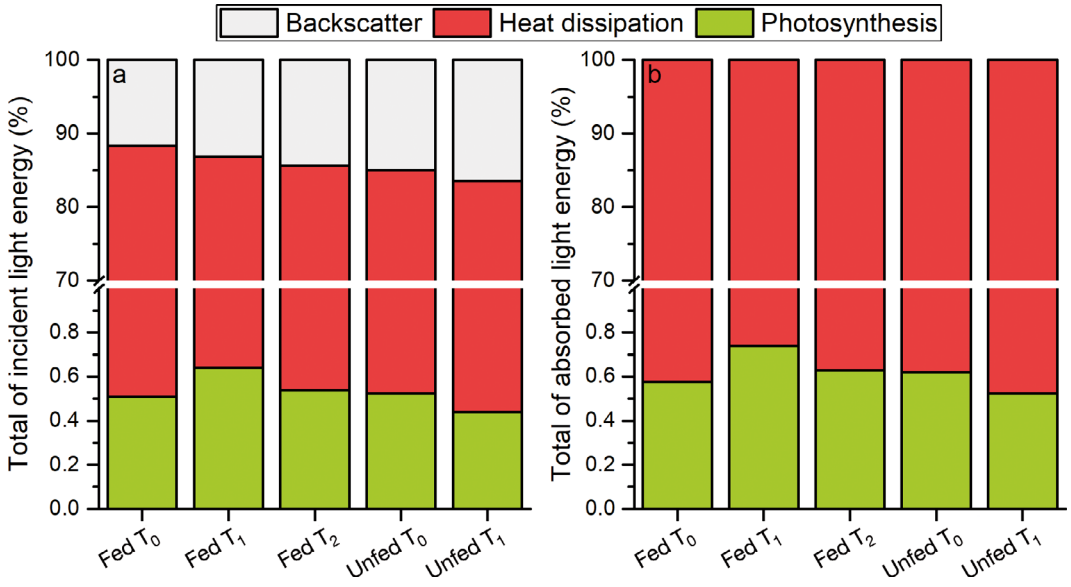

Fig. 9. Radiative energy budget of fed and unfed *Pocillopora* sp. under thermal stress in percent of (a) total incident and (b) total absorbed light energy under high downwelling photon irradiance of 2400 µmol photons m^{-2} s^{-1}. Gray bars indicate the amount of reflected light energy, red bars indicate the amount of light energy dissipated as heat, and green bars indicate amount of light energy conserved by photosynthesis. Note breaks in *y*-axes

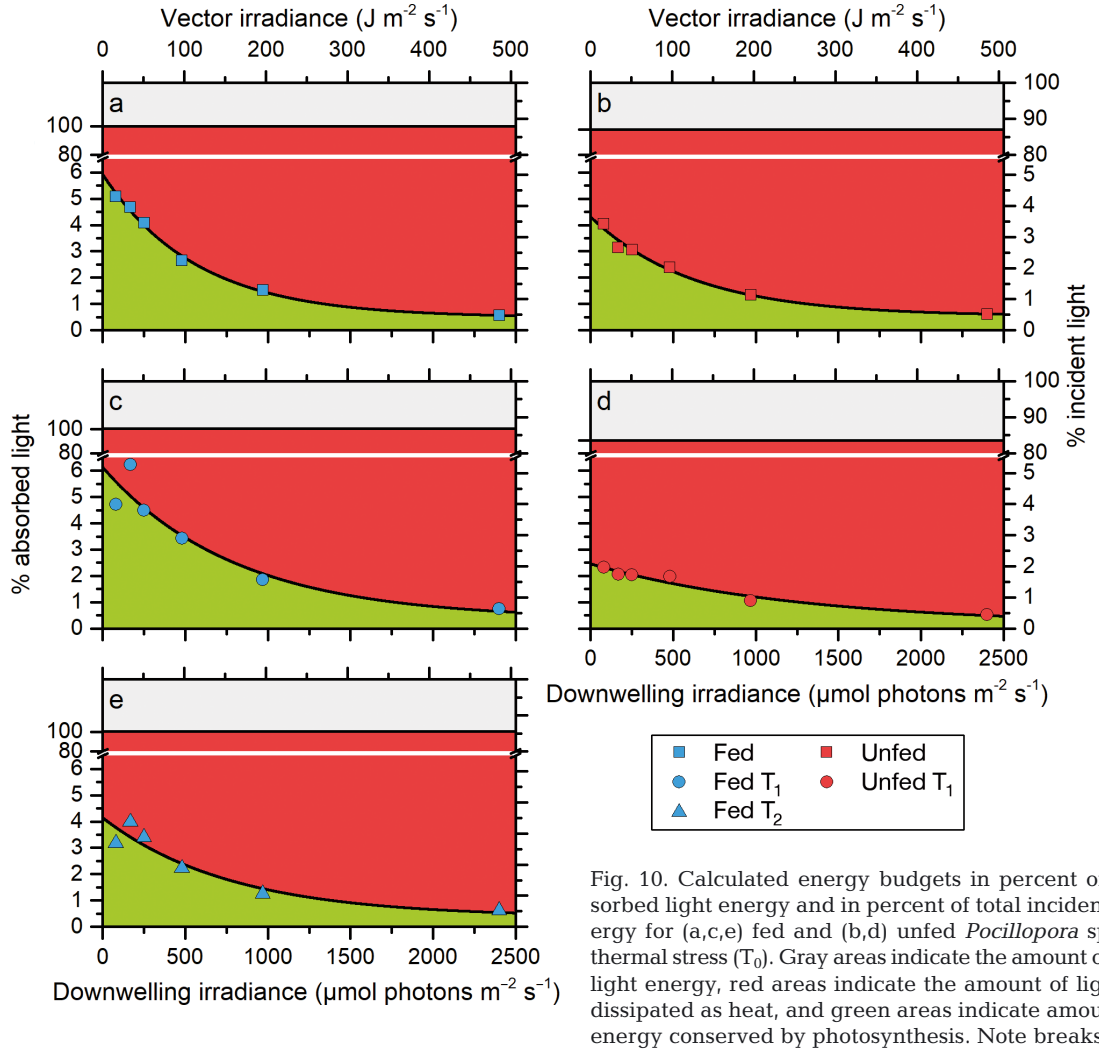

Fig. 10. Calculated energy budgets in percent of total absorbed light energy and in percent of total incident light energy for (a,c,e) fed and (b,d) unfed *Pocillopora* sp. without thermal stress (T_0). Gray areas indicate the amount of reflected light energy, red areas indicate the amount of light energy dissipated as heat, and green areas indicate amount of light energy conserved by photosynthesis. Note breaks in *y*-axes

fed fragments of *Pocillopora* sp., the highest amount of photosynthetic energy use, i.e. about 5–6% of absorbed irradiance, was found at 80 µmol photons m^{-2} s^{-1}, while unfed *Pocillopora* sp. reached about 4% at T_0. Corals from both treatments experienced an exponential decrease in photosynthetic energy quenching at higher irradiances and reached the lowest amount of 0.5% for fed and 0.6% for unfed at 2400 µmol photons m^{-2} s^{-1}. Photosynthetic use of absorbed light decreased to about 2.5% of absorbed light energy for unfed fragments after 3 d of thermal stress (T_1), while fed fragments remained unaffected by thermal stress for 8 d (T_2) before photosynthetic energy quenching dropped to about 4% (Fig. 10).

4. DISCUSSION

In this study, we present the first comparison of closed radiative energy budgets for heterotrophically fed and unfed specimens of the symbiont-bearing coral *Pocillopora* sp. We investigated changes in ratios of photosynthesis and heat generation related to thermal stress and found that although both fed and unfed corals responded to thermal stress by bleaching, fed *Pocillopora* sp. appeared more resilient to thermal stress, as they were able to remain photosynthetically competent for 5 d longer than unfed specimens.

4.1. Photosynthesis and thermal stress

When comparing across all time points, the areal gross photosynthesis in fed corals was about 1.2 times higher than in unfed corals (Fig. 6a). Furthermore, both relative electron transport rate (rETR) and the effective quantum yield of PSII [*Y*(II)] were higher at all irradiance levels in fed relative to unfed corals pre- and post-bleaching (Fig. 2), which is similar to previous studies (e.g. Ferrier-Pagès et al. 2010). Feeding corals has been shown to alleviate photodamage of symbiotic dinoflagellates, where unfed corals showed a decline in their nocturnal recovery rates of PSII relative to fed corals, and thus suffered more from chronic photoinhibition (Borell & Bischof 2008, Borell et al. 2008).

Additionally, both rETR and *Y*(II) in fed corals increased with thermal stress (T_2; Fig. 2), which stands in contrast to the results from previous studies (e.g. Ferrier-Pagès et al. 2010). Thermal stress usually inhibits the photosynthetic capabilities of aquatic phototrophs, as increased temperature leads to degradation of enzymes crucial for sustaining electron transport in the photosystems (Falkowski & Raven 2007). However, our corals showed little to no decline in photosynthetic rates when exposed to thermal stress, and cell-specific photosynthesis rates of *Cladocopium* sp. actually increased in both fed and unfed corals (Fig. 6b). While this measured increase in rETR and *Y*(II) remains unclear, we speculate that several factors have impacted the performance of individual cells leading to an overall short-term enhancement of their photosynthetic performance. Although symbiont densities steadily decreased under thermal stress (Fig. 3a), the chlorophyll content per cell and areal gross photosynthesis did not significantly change pre- and post-bleaching in the individual feeding treatment (Figs. 3c & 6a). High dinoflagellate cell densities (>1 × 10^6 cells cm^{-2}) can lead to algal self-shading (Enriquez et al. 2005), and thus reduce photosynthesis in deeper tissue layers due to high light attenuation. Loss of dinoflagellates during coral bleaching can initially alleviate such self-shading effects, leading to enhanced light availability with fewer symbiont cells and potential higher photosynthetic rates (Enriquez et al. 2005). Such light enhancement was demonstrated in our scalar irradiance measurements at the coral tissue surface, which increased from ~120–130% of the incident downwelling irradiance for both fed and unfed corals pre-bleaching (T_0) up to ~140–145% of incident downwelling irradiance at the coral tissue surface after 3 d of thermal stress (T_1; Fig. 4a). Such enhancement of scalar irradiance in coral tissue surface is common in bleached corals, and enhancements of up to 200% have previously been measured in polyp surface tissue of bleached *Pocillopora* sp. (Wangpraseurt et al. 2017a). Although the thin tissue of *Pocillopora* sp. did not exhibit strong light gradients compared to more thick-tissued corals (Wangpraseurt et al. 2012), the scalar irradiance at the tissue–skeleton interface in polyp corallites was slightly lower compared to surface layers (95% of incident irradiance in fed, and 110% in unfed, T_0; Fig. 4b). This attenuation became even more apparent post-bleaching, as scalar irradiance at the tissue–skeleton interface in corals from both treatments further decreased (100% in unfed T_1 and 78% in fed T_2; Fig. 4b). The reduced light attenuation during bleaching could be caused by the presence of endolithic microbes residing in the coral skeleton decreasing skeleton backscatter in certain regions of the light spectrum (Fig. 4; compare T_1 in panels c and f, and T_2 in panels b and d; Fork & Larkum 1989, Magnusson et al.(2007). However, no such endoliths appeared present to the naked eye,

and the role of endolithic phototrophs was not further investigated.

Local enhancement in scalar irradiance at the coral tissue surface, and thus alleviation of self-shading, increased cell-specific photosynthetic rates by about a factor of 1.1 in unfed corals, and 1.5 in fed corals, after thermal stress (T_1–T_2 relative to T_0; Fig. 6b). However, areal gross photosynthesis differed between the 2 feeding treatments, showing an initial increase for fed corals (T_1), while unfed corals showed immediate signs of thermal stress with lowered areal gross photosynthesis (compare T_1 in fed and unfed, Fig. 6a).

Furthermore, since *Cladocopium* sp. in unfed corals barely showed any increase in cell-specific photosynthetic rate (Fig. 6b), this may indicate that resource limitation pushed the unfed corals to their metabolic threshold with few resources to spare, in contrast to fed corals. This could explain the increased rETR and *Y*(II) found only in fed corals. Alleviation of self-shading was also evident from photosynthesis versus photon irradiance curves for fed corals, where P_{max} remained constant (~0.50–0.52 nmol O_2 cm^{-2} s^{-1}) between thermal treatments (T_2 relative to T_0), while the α-value was considerably decreased after thermal stress (Fig. 7a). With P_{max} staying constant before and after thermal stress in fed corals, this indicates that fed corals were able to maintain their photosynthetic maximum but needed more light because of a decreased light utilization efficiency (α-value decreased).

4.2. Temperature microenvironment

Corals from either feeding treatment did not express any significant changes in radiative surface tissue warming (ΔT) as a result of thermal stress (Fig. 8b). However, variable chlorophyll fluorescence imaging data of fed corals did reveal a clear decrease in NPQ after 8 d at 30°C (T_2) relative to the control corals (T_0, Fig. S2). Spectral reflectance was increased for bleached corals, thus reducing the amount of absorbed light energy and coral surface warming (Enriquez et al. 2005, Jimenez et al. 2012). We found the same trend of spectral reflectance steadily increasing with thermal stress in corals from both feeding treatments (Fig. 5), along with a clear negative correlation between coral spectral reflectance and symbiont density (R^2 = 0.99; Fig. S4). As such, the decrease in surface tissue heat exchange can be explained by the observed steady decrease in symbiont density and chlorophyll content during thermal stress (Fig. 3).

4.3. Radiative energy budgets

To establish radiative energy budgets for corals, we required a distinct thermal boundary layer that was not clearly observable below a photon irradiance of 2400 µmol photons m^{-2} s^{-1} due to lower tissue surface heating at lower incident light energy. At such high irradiance, we observed that regardless of feeding status and thermal stress, all corals exhibited a similar energy budget where only about 85–88% of the incident light was absorbed, and furthermore that in all cases >99% of the absorbed light energy was dissipated as heat (Fig. 9). Since our corals were acclimated to a photon irradiance (400–700 nm) of ~250 µmol photons m^{-2} s^{-1}, we estimated theoretical radiative energy budgets calculated from photosynthesis data acquired at lower light levels (see Section 2.6).

Extrapolation of the radiative energy budget to lower incident irradiances showed that photosynthesis could account for up to ~4 and ~5–6% of absorbed light energy in non-stressed (T_0) unfed and fed corals, respectively, under light-limiting conditions (Fig. 10a,b). In a previous study on a massive symbiont-bearing coral, Brodersen et al. (2014) showed that a non-stressed *Montastrea curta* performed slightly better in terms of light energy efficiency as compared to the *Pocillopora* sp. investigated in this study. *M. curta* had a maximum photosynthetic energy efficiency of ~4% at 640 µmol photons m^{-2} s^{-1} under a flow velocity of 0.4 cm s^{-1}, while our fed *Pocillopora* sp. only reached a photosynthetic energy efficiency of ~2% under a similar irradiance and a slightly slower flow velocity of 0.25 cm s^{-1}. The difference in photosynthetic efficiency between *Pocillopora* sp. and *M. curta* might be due to differences in skeletal heat conduction (Jimenez et al. 2012), as thin-tissued branching corals such as *Pocillopora* sp. exhibit a higher heat conduction into the skeleton than thick-tissued massive corals. TBL measured on *Pocillopora* sp. with a temperature microsensor revealed an average TBL thickness of ~680 µm, whereas Brodersen et al. (2014) found a TBL thickness of >3 mm for *M. curta* at similar flow conditions. The TBL thickness is controlled by coral growth form and microtopography (Jimenez et al. 2008). The small-polyped *Pocillopora* sp. has a rather smooth tissue surface structure compared to massive faviid corals (Wangpraseurt et al. 2017b), thus explaining the relatively thin TBL found in *Pocillopora* sp. (Jimenez et al. 2011). The highly complex topography and tissue organization of corals thus play a key role for the radiative energy budget and photosynthetic efficiency of corals (Lichtenberg et al. 2016). In contrast, studies on energy use

efficiency in other highly pigmented photosynthetic systems (e.g. benthic biofilms and coral sediments) reveal low energy use efficiencies due to their more uniform topography and high optical density (Al-Najjar et al. 2010, Lichtenberg et al. 2017).

Clear differences in thermal tolerance were observed from our calculated energy budgets at lower irradiance (80–250 µmol photons m^{-2} s^{-1}). Fed corals appeared unaffected by the temperature increase 3 d after the onset of thermal stress, whereas unfed corals expressed an immediate sign of stress via decreased photosynthetic quenching of absorbed light energy (4 % as compared to 2–2.5 %; Fig. 10d). Only after an additional 5 d of thermal stress did fed corals also express signs of stress by decreasing their photosynthetic quenching of absorbed light energy from 5–6 % down to ~4 % (Fig. 10e). Such differences in thermal tolerance can have important ecological implications, since corals located in nutrient-rich environments will be more resilient to stress compared to corals growing in oligotrophic nutrient-poor environments.

We conclude that actively feeding *Pocillopora* sp. handled thermal stress better and maintained their energy demand, as the remaining symbionts showed increased photosynthetic rates during bleaching. How such implications of feeding behavior, symbiont densities, and photosynthesis relate to real-world thermal stress events is yet to be determined.

Acknowledgements. We thank the staff at the Scientific Center of Monaco for their excellent assistance with experimental procedures, and labor-intensive general maintenance and care of the corals for the duration of this study. The study was funded by grants from the Carlsberg Foundation (D.W., M.K.), the European Union's Horizon 2020 scheme (D.W.), a Sapere Aude Advanced Grant from the Independent Research Fund Denmark (M.K.; DFF-1323-00065B), and the Scientific Center of Monaco (part of the RTPI Nutress).

LITERATURE CITED

Ainsworth TD, Heron SF, Ortiz JC, Mumby PJ and others (2016) Climate change disables coral bleaching protection on the Great Barrier Reef. Science 352:338–342

Al-Najjar MA, de Beer D, Jorgensen BB, Kühl M, Polerecky L (2010) Conversion and conservation of light energy in a photosynthetic microbial mat ecosystem. ISME J 4: 440–449

Al-Najjar MA, de Beer D, Kühl M, Polerecky L (2012) Light utilization efficiency in photosynthetic microbial mats. Environ Microbiol 14:982–992

Anthony KRN, Hoegh-Guldberg O (2003) Variation in coral photosynthesis, respiration and growth characteristics in contrasting light microhabitats: an analogue to plants in forest gaps and understoreys? Funct Ecol 17:246–259

Baker NR (2008) Chlorophyll fluorescence: a probe of photosynthesis in vivo. Annu Rev Plant Biol 59:89–113

Borell EM, Bischof K (2008) Feeding sustains photosynthetic quantum yield of a scleractinian coral during thermal stress. Oecologia 157:593–601

Borell EM, Yuliantri AR, Bischof K, Richter C (2008) The effect of heterotrophy on photosynthesis and tissue composition of two scleractinian corals under elevated temperature. J Exp Mar Biol Ecol 364:116–123

Bou-Abdallah F, Chasteen ND, Lesser MP (2006) Quenching of superoxide radicals by green fluorescent protein. Biochim Biophys Acta 1760:1690–1695

Bourne DG, Garren M, Work TM, Rosenberg E, Smith GW, Harvell CD (2009) Microbial disease and the coral holobiont. Trends Microbiol 17:554–562

Brodersen KE, Lichtenberg M, Ralph PJ, Kühl M, Wangpraseurt D (2014) Radiative energy budget reveals high photosynthetic efficiency in symbiont-bearing corals. J R Soc Interface 11:20130997

Brown BE, Dunne RP (2015) Coral bleaching: the roles of sea temperature and solar radiation. In: Woodley CM, Downs CA, Bruckner AW, Porter JW, Galloway SB (eds) Diseases of coral. John Wiley & Sons, Hoboken, NJ, p 266–283

Chan NCS, Wangpraseurt D, Kühl M, Connolly SR (2016) Flow and coral morphology control coral surface pH: implications for the effects of ocean acidification. Front Mar Sci 3:10

Edmunds PJ, Davies PS (1989) An energy budget for *Porites porites* (Scleractinia), growing in a stressed environment. Coral Reefs 8:37–43

Enriquez S, Mendez ER, Iglesias-Prieto R (2005) Multiple scattering on coral skeletons enhances light absorption by symbiotic algae. Limnol Oceanogr 50:1025–1032

Falkowski PG, Raven JA (2007) Aquatic photosynthesis, 2nd edn., Princeton University Press, Princeton, NJ

Ferrier-Pagès C, Rottier C, Beraud E, Levy O (2010) Experimental assessment of the feeding effort of three scleractinian coral species during a thermal stress: effect on the rates of photosynthesis. J Exp Mar Biol Ecol 390:118–124

Fork DC, Larkum AWD (1989) Light harvesting in the green-alga *Ostreobium* sp., a coral symbiont adapted to extreme shade. Mar Biol 103:381–385

Gittins JR, D'Angelo C, Oswald F, Edwards RJ, Wiedenmann J (2015) Fluorescent protein-mediated colour polymorphism in reef corals: multicopy genes extend the adaptation/acclimatization potential to variable light environments. Mol Ecol 24:453–465

Glynn PW (1996) Coral reef bleaching: facts, hypotheses and implications. Glob Change Biol 2:495–509

Hill R, Schreiber U, Gademann R, Larkum AWD, Kühl M, Ralph PJ (2004) Spatial heterogeneity of photosynthesis and the effect of temperature-induced bleaching conditions in three species of corals. Mar Biol 144:633–640

Hill R, Brown CM, DeZeeuw K, Campbell DA, Ralph PJ (2011) Increased rate of D1 repair in coral symbionts during bleaching is insufficient to counter accelerated photo-inactivation. Limnol Oceanogr 56:139–146

Hoegh-Guldberg O (1999) Climate change, coral bleaching and the future of the world's coral reefs. Mar Freshw Res 50:839–866

Hoegh-Guldberg O, Mumby PJ, Hooten AJ, Steneck RS and others (2007) Coral reefs under rapid climate change and ocean acidification. Science 318:1737–1742

Houlbrèque F, Ferrier-Pagès C (2009) Heterotrophy in tropical scleractinian corals. Biol Rev Camb Philos Soc 84: 1–17

Hughes TP, Baird AH, Bellwood DR, Card M and others (2003) Climate change, human impacts, and the resilience of coral reefs. Science 301:929–933

Hughes TP, Kerry JT, Álvarez-Noriega M, Álvarez-Romero JG and others (2017) Global warming and recurrent mass bleaching of corals. Nature 543:373–377

Jeffrey SW, Humphrey GF (1975) New spectrophotometric equations for determining chlorophylls *a*, *b*, c_1 and c_2 in higher plants, algae and natural phytoplankton. Biochem Physiol Pflanz 167:191–194

Jimenez IM, Kühl M, Larkum AWD, Ralph PJ (2008) Heat budget and thermal microenvironment of shallow-water corals: Do massive corals get warmer than branching corals? Limnol Oceanogr 53:1548–1561

Jimenez IM, Kühl M, Larkum AW, Ralph PJ (2011) Effects of flow and colony morphology on the thermal boundary layer of corals. J R Soc Interface 8:1785–1795

Jimenez IM, Larkum AWD, Ralph PJ, Kühl M (2012) Thermal effects of tissue optics in symbiont-bearing reef-building corals. Limnol Oceanogr 57:1816–1825

Kaandorp JA, Lowe CP, Frenkel D, Sloot PM (1996) Effect of nutrient diffusion and flow on coral morphology. Phys Rev Lett 77:2328–2331

Kühl M, Cohen Y, Dalsgaard T, Jørgensen BB, Revsbech NP (1995) Microenvironment and photosynthesis of zooxanthellae in scleractinian corals studied with microsensors for O_2, pH and light. Mar Ecol Prog Ser 117:159–172

LaJeunesse TC, Parkinson JE, Gabrielson PW, Jeong HJ, Reimer JD, Voolstra CR, Santos SR (2018) Systematic revision of Symbiodiniaceae highlights the antiquity and diversity of coral endosymbionts. Curr Biol 28:2570–2580

Lesser MP (1996) Elevated temperatures and ultraviolet radiation cause oxidative stress and inhibit photosynthesis in symbiotic dinoflagellates. Limnol Oceanogr 41: 271–283

Lesser MP, Farrell JH (2004) Exposure to solar radiation increases damage to both host tissues and algal symbionts of corals during thermal stress. Coral Reefs 23:367–377

Lesser MP, Weis VM, Patterson MR, Jokiel PL (1994) Effects of morphology and water motion on carbon delivery and productivity in the reef coral, *Pocillopora damicornis* (Linnaeus): diffusion barriers, inorganic carbon limitation, and biochemical plasticity. J Exp Mar Biol Ecol 178: 153–179

Lichtenberg M, Larkum AWD, Kühl M (2016) Photosynthetic acclimation of *Symbiodinium* in hospite depends on vertical position in the tissue of the scleractinian coral *Montastrea curta*. Front Microbiol 7:230

Lichtenberg M, Brodersen KE, Kühl M (2017) Radiative energy budgets of phototrophic surface-associated microbial communities and their photosynthetic efficiency under diffuse and collimated light. Front Microbiol 8:452

Lyndby NH, Kühl M, Wangpraseurt D (2016) Heat generation and light scattering of green fluorescent protein-like pigments in coral tissue. Sci Rep 6:26599

Magnusson SH, Fine M, Kühl M (2007) Light microclimate of endolithic phototrophs in the scleractinian corals *Montipora monasteriata* and *Porites cylindrica*. Mar Ecol Prog Ser 332:119–128

Marcelino LA, Westneat MW, Stoyneva V, Henss J and others (2013) Modulation of light-enhancement to symbiotic algae by light-scattering in corals and evolutionary trends in bleaching. PLOS ONE 8:e61492

Muscatine L, McCloskey LR, Marian RE (1981) Estimating the daily contribution of carbon from zooxanthellae to coral animal respiration. Limnol Oceanogr 26:601–611

Odum HT, Odum EP (1955) Trophic structure and productivity of a windward coral reef community on Eniwetok Atoll. Ecol Monogr 25:291–320

Ralph PJ, Schreiber U, Gademann R, Kühl M, Larkum AWD (2005) Coral photobiology studied with a new imaging pulse amplitude modulated fluorometer. J Phycol 41: 335–342

Revsbech NP, Jørgensen BB (1983) Photosynthesis of benthic microflora measured with high spatial resolution by the oxygen microprofile method: capabilities and limitations of the method. Limnol Oceanogr 28:749–756

Rickelt LF, Lichtenberg M, Trampe ECL, Kühl M (2016) Fiber-optic probes for small-scale measurements of scalar irradiance. Photochem Photobiol 92:331–342

Rodolfo-Metalpa R, Richard C, Allemand D, Bianchi CN, Morri C, Ferrier-Pagès C (2006) Response of zooxanthellae in symbiosis with the Mediterranean corals *Cladocora caespitosa* and *Oculina patagonica* to elevated temperatures. Mar Biol 150:45–55

Thornhill DJ, Rotjan RD, Todd BD, Chilcoat GC and others (2011) A connection between colony biomass and death in Caribbean reef-building corals. PLOS ONE 6:e29535

Veal CJ, Carmi M, Dishon G, Sharon Y and others (2010a) Shallow-water wave lensing in coral reefs: a physical and biological case study. J Exp Biol 213:4304–4312

Veal CJ, Holmes G, Nunez M, Hoegh-Guldberg O, Osborn J (2010b) A comparative study of methods for surface area and three-dimensional shape measurement of coral skeletons. Limnol Oceanogr Methods 8:241–253

Wangpraseurt D, Larkum AW, Ralph PJ, Kühl M (2012) Light gradients and optical microniches in coral tissues. Front Microbiol 3:316

Wangpraseurt D, Larkum AW, Franklin J, Szabo M, Ralph PJ, Kühl M (2014a) Lateral light transfer ensures efficient resource distribution in symbiont-bearing corals. J Exp Biol 217:489–498

Wangpraseurt D, Tamburic B, Szabo M, Suggett D, Ralph PJ, Kühl M (2014b) Spectral effects on *Symbiodinium* photobiology studied with a programmable light engine. PLOS ONE 9:e112809

Wangpraseurt D, Holm JB, Larkum AW, Pernice M, Ralph PJ, Suggett DJ, Kühl M (2017a) *In vivo* microscale measurements of light and photosynthesis during coral bleaching: evidence for the optical feedback loop? Front Microbiol 8:59

Wangpraseurt D, Wentzel C, Jacques SL, Wagner M, Kühl M (2017b) *In vivo* imaging of coral tissue and skeleton with optical coherence tomography. J R Soc Interface 14: 20161003

Wangpraseurt D, Jacques S, Lyndby NH, Holm JB, Ferrier-Pagès C, Kühl M (2019) Microscale light management and inherent optical properties of intact corals studied with optical coherence tomography. J R Soc Interface 16: 20180567

Webb WL, Newton M, Starr D (1974) Carbon dioxide exchange of *Alnus rubra*. Oecologia 17:281–291

Welch AJ, van Gemert MJC (2011) Optical-thermal response of laser-irradiated tissue. Springer, New York, NY

Wiedenmann J, D'Angelo C, Smith EG, Hunt AN, Legiret FE, Postle AD, Achterberg EP (2013) Nutrient enrichment can increase the susceptibility of reef corals to bleaching. Nat Clim Chang 3:160–164

Editorial responsibility: Joseph Pawlik, Wilmington, North Carolina, USA

Submitted: July 23, 2018; Accepted: September 30, 2019
Proofs received from author(s): October 21, 2019